MEASUREMENT OF PHASE SPACE DENSITY EVOLUTION IN MICE

F. Drielsma[*], Université de Genève, Geneva, Switzerland

D. Maletic[†], Institute of Physics Belgrade, Belgrade, Serbia

Abstract

The Muon Ionization Cooling Experiment (MICE) collaboration will demonstrate the feasibility of ionization cooling, the technique by which it is proposed to cool the muon beam at a future neutrino factory or muon collider. The position and momentum reconstruction of individual muons in the MICE trackers allows for the development of alternative figures of merit in addition to beam emittance. Contraction of the phase space volume occupied by a fraction of the sample, or equivalently the increase in phase space density at its core, is an unequivocal cooling signature. Single-particle amplitude and nonparametric statistics provide reliable methods to estimate the phase space density function. These techniques are robust to transmission losses and non-linearities, making them optimally suited to perform a quantitative cooling measurement in MICE.

INTRODUCTION

Future facilities such as the Muon Collider and the Neutrino Factory will require high intensity and low emittance stored muon beams [1, 2]. Muons are produced as tertiary particles ($p + N \rightarrow \pi + X$, $\pi \rightarrow \mu + \nu$) inheriting a large emittance from the isotropic decay of the pions. For efficient acceleration, the phase space volume of these beams must be reduced significantly, i.e. "cooled", to fit within the acceptance of a storage ring or accelerator beam pipe. Due to the short muon lifetime, ionization cooling is the only practical and efficient technique to cool muon beams [3, 4]. Each muon in the beam loses momentum in all dimensions through ionization energy loss in an absorbing material, reducing the RMS emittance and increasing its phase space density. Subsequent acceleration though radio frequency cavities restores longitudinal energy, resulting in a beam with reduced transverse emittance. A factor of close to 10^6 in reduced 6D emittance has been achieved in simulation with a 970 m long channel [5]. The rate of change in normalized transverse RMS emittance, ϵ_N, is given by the ionization cooling equation [3]:

$$\frac{d\varepsilon_N}{ds} \simeq -\frac{\varepsilon_N}{\beta^2 E_\mu}\left|\frac{dE_\mu}{ds}\right| + \frac{\beta_\perp (13.6\,\text{MeV})^2}{2\beta^3 E_\mu m_\mu c^2 X_0}, \qquad (1)$$

where βc is the muon velocity, $|dE/ds|$ is the average rate of energy loss, E_μ and $m\mu$ are the muon energy and mass, $\beta_\perp$ is the transverse betatron function and X_0 is the radiation length of the absorber material. The first term on the right can be referred to as the "cooling" term driven by energy loss, while the second term is the "heating term" that uses the PDG approximation for the multiple Coulomb scattering.

MICE [6] is currently taking data in the Step IV configuration in order to make detailed measurements of the scattering, energy loss [7] and phase space evolution at different momenta and channel configurations, with lithium hydride and liquid hydrogen absorbers. A schematic drawing of MICE Step IV is shown in Figure 1. MICE consists of two scintillating fiber trackers upstream and downstream of the absorber in strong solenoid fields to accurately reconstruct the position and the momentum of individual muons selected in a series of particle identification detectors, including 3 time-of-flight hodoscopes (ToF0/1/2), 2 threshold Cherenkov counters, a pre-shower calorimeter (KL) and a fully active tracker-calorimeter (EMR) [8–11].

COOLING CHANNEL

The two spectrometer solenoid modules each generate a region of uniform 3 T field in which diagnostic trackers are situated and a matching region that transports the beam from the solenoid to the focus coil module. The focus coil module, positioned between the solenoids, provides additional focusing to increase the angular divergence of the beam at the absorber, improving the amount of emittance reduction that can be achieved. The magnetic field model is shown in Figure 2. The absorber was a single 65 mm thickness lithium hydride disk. Lithium hydride was chosen as an absorber material as it provides less multiple Coulomb scattering for a given energy loss.

In this paper the evolution of phase space density is reported for a single configuration of the cooling apparatus. Results from one transfer line configuration are reported, with the accumulated muon sample having a nominal emittance of 6 mm at momenta around 140 MeV/c in the upstream spectrometer solenoid, denoted as '6–140'.

As MICE measures each particle event individually, it is possible to select a particle ensemble from the collection of measured tracks. This enables the study of momentum spread and transverse beam parameters on the cooling. In this analysis, muons have been selected with:

- longitudinal momentum in the range 135 to 145 MeV/c;

- time-of-flight between TOF0 and TOF1 consistent with muons in this momentum range; and

- a single, good quality track formed in the upstream diagnostics.

In order to study the evolution of the phase space density through the whole cooling channel and across the absorber, a realistic simulation of the setting of interest was produced. The betatron function of the selected muon ensemble is shown for the Monte Carlo (MC) simulation, the

---

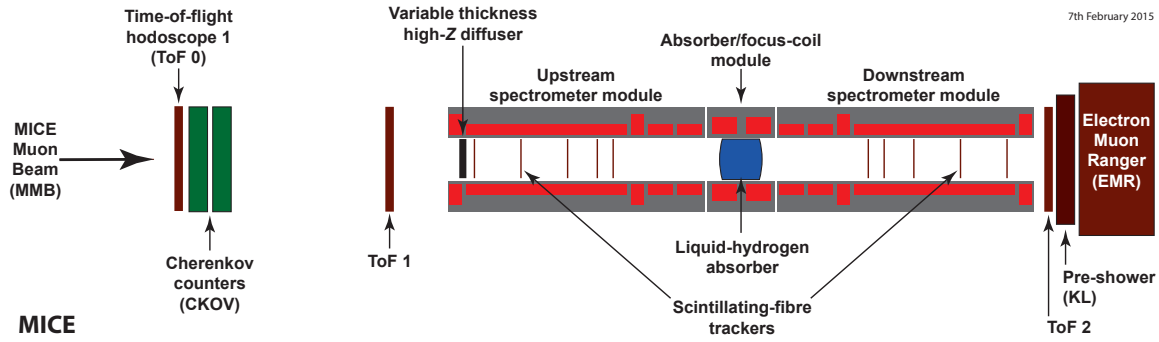[*] francois.drielsma@unige.ch

[†] Speaker

MOA13

Figure 1: Layout of the MICE Step IV configuration, its absorber module, tracking spectrometers and PID detectors.
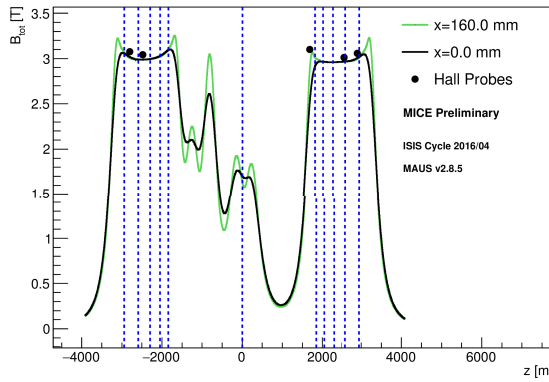

Figure 2: Modelled magnetic field for the configuration on the axis and with 160 mm horizontal displacement from the axis. Hall probes, situated 160 mm from the beam axis, show a 2 % discrepancy with the model. Dashed lines show position of the tracker stations and absorber (at $z = 0$).

reconstructed MC and the data for the '6–140' setting in Figure 3. The graph shows a large growth of the beam size in the downstream section due to the absence of the downstream match coils in this configuration. The simulation closely reproduces the function measured in the data.
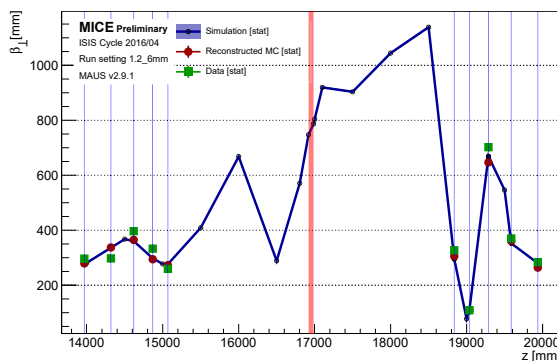

Figure 3: Beta function profile in the MC truth (blue line), reconstructed MC (red circles) and data (green squares).

PHASE SPACE DENSITY EVOLUTION

Emittance

The transverse normalized RMS emittance is the most common cooling figure of merit and is defined as

$$\epsilon_N = \frac{1}{m_\mu} |\Sigma|^{\frac{1}{4}}, \qquad (2)$$

with m_μ the muon mass and $|\Sigma|$ the determinant of the 4D transverse phase space covariance matrix, i.e. $\Sigma_{ij} = \langle ij \rangle - \langle i \rangle \langle j \rangle$ with $i, j \in [x, p_x, y, p_y]$. For a Gaussian beam, this quantity is directly related to the volume of the $1\,\sigma$ RMS ellipse, V_{RMS}, through $\epsilon_N = \sqrt{2V_{RMS}}/(m\pi)$.

In a fully transmitted beam, emittance reduction is a clean signature of the contraction of transverse phase space volume. For a partially scraped beam, as shown for the '6–140' setting in Figure 4, the emittance evolution exhibits apparent emittance reduction in the downstream section due to the loss of the tails of the distribution. It also experiences significant apparent growth in the downstream tracker due to high field gradient, causing filamentation in the beam.
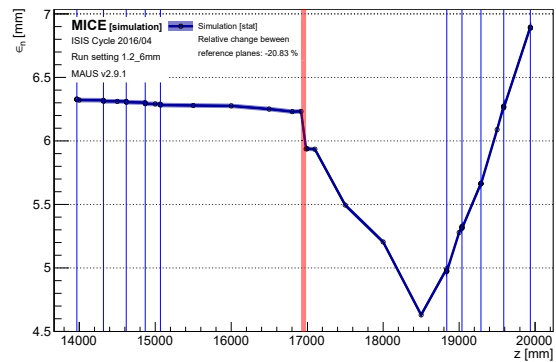

Figure 4: Normalized transverse RMS emittance evolution through the MICE cooling channel.

An alternative to RMS emittance is to study the evolution of the density distribution of the ensemble, as it allows for the selection of a defined and identical fraction of phase space upstream and downstream of the absorber.

Amplitude

The 4D amplitude of a particle with phase space vector $\mathbf{v} = (x, p_x, y, p_y)$ is given by

$$A_\perp = \epsilon_N (\mathbf{v} - \boldsymbol{\mu})^T \Sigma^{-1} (\mathbf{v} - \boldsymbol{\mu}). \tag{3}$$

with $\boldsymbol{\mu} = (\langle x \rangle, \langle p_x \rangle, \langle y \rangle, \langle p_y \rangle)$, the beam centroid. In order to prevent the tails of the distribution from skewing the core, only those events with amplitude less than $A_\perp$ have been included in the calculation of $\boldsymbol{\mu}$ and Σ for a given event. The high amplitude particles are iteratively removed from the sample first as they are calculated.

The distribution of muons is represented in Figure 5 in the tracker station that is furthest downstream in the (x, p_x) projection. The color of the points in the scatter plot represents the amplitude of the particle at that position. The distribution exhibits a clear Gaussian core of low amplitudes, while the tails are easily identified as high amplitude points.
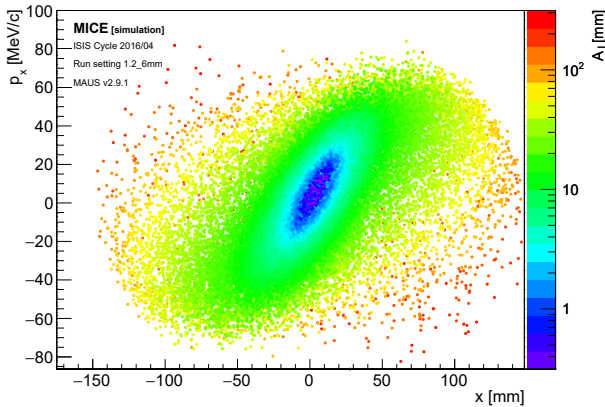

Figure 5: Scatter plot of the particles in the tracker station that is furthest downstream in the (x, p_x) projection. The color scale represents the individual particle amplitudes.

The amplitude of a particle in a Gaussian beam is related to its local density through

$$\rho(\mathbf{v}) = \frac{1}{4\pi^2 m^2 \epsilon_N^2} \exp \left[-\frac{A_\perp}{2\epsilon_N} \right]. \tag{4}$$

A low amplitude sample corresponds to the high density core of the beam.

Subemittance

The α-subemittance, e_α, is defined as the RMS emittance of the core fraction α of the parent beam. For a truncated 4D Gaussian beam of covariance S, it satisfies

$$\frac{e_\alpha}{\epsilon_N} = \frac{|S|^{\frac{1}{4}}}{|\Sigma|^{\frac{1}{4}}} = \frac{1}{2\alpha} \gamma \left(3, Q_{\chi_4^2}^2(\alpha)/2 \right), \tag{5}$$

with $\gamma(\cdot, \cdot)$ the lower incomplete gamma function and $Q_{\chi_4^2}(\cdot)$, the 4-degrees-of-freedom χ^2 distribution quantiles.

If an identical fraction α of the input beam is selected upstream and downstream, i.e. the same amount of particles, the measured subemittance change is identical to the normalized RMS emittance change. The evolution of the 9 %-subemittance is represented in Figure 6. The choice of 9 % is natural in four dimensions as it represents the fraction contained within the 4D RMS ellipsoid of a 4-variate Gaussian. This quantity exhibits a clean cooling signal across the absorber that is unaltered by transmission losses and nonlinearities. The only trade-off is that the relative statistical error on α-subemittance grows as $\alpha^{-\frac{1}{2}}$. The estimated relative emittance change with this technique is -7.54 ± 1.25 %, compatible with predictions.
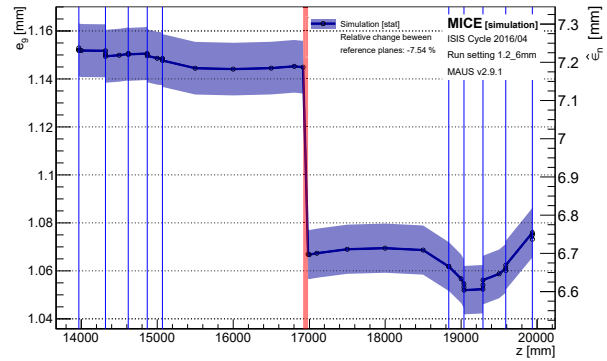

Figure 6: 9 %-subemittance evolution through the MICE cooling channel.

Fractional Emittance

The α-fractional emittance, ϵ_α, is defined as the phase space volume occupied by the core fraction α of the parent beam. For a truncated 4D Gaussian beam, it satisfies

$$\epsilon_\alpha = \frac{1}{2} m^2 \pi^2 \epsilon_N^2 Q_{\chi_4^2}^2(\alpha). \tag{6}$$

This volume scales as function of α only and is proportional to the square of the normalized emittance. For a relative emittance change $\delta = \Delta\epsilon_N / \epsilon_N^{up}$, one yields

$$\frac{\Delta\epsilon_\alpha}{\epsilon_\alpha^{up}} = \delta(2 + \delta) \simeq 2\frac{\Delta\epsilon_N}{\epsilon_N^{up}}. \tag{7}$$

The last approximation holds for small fractional changes. The volume of a fraction α of the beam is reconstructed by taking the convex hull of the selected ensemble [12]. Figure 7 shows the evolution of the 9 %-fractional emittance. The estimated relative emittance change with this technique is -7.85 ± 1.08 %.

Nonparametric Density Estimation

Nonparametric statistics are not based on parameterized families of probability distributions. Unlike parametric density estimation, such as amplitude, nonparametric statistics
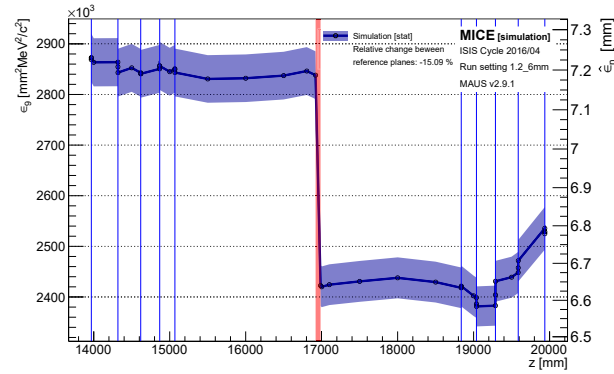
Figure 7: 9 %-fractional emittance evolution through the MICE cooling channel.

make no assumptions about the probability distributions of the variables being assessed.

There are many classes of estimators that have been developed in the last century. Three of them have been considered in this study: optimally binned histograms, k-Nearest Neighbors (kNN) and Tessellation Density Estimators (TDEs) [13–16]. Systematic studies showed that the kNN method is the most efficient and robust technique in four dimensions. For a given phase space vector $\mathbf{v} = (x, p_x, y, p_y)$, find the k nearest points in the input cloud, calculate the distance to the kth nearest neighbor, R_k, and evaluate the density as

$$\rho(\mathbf{v}) = \frac{k}{V_k} = \frac{k\Gamma\left(\frac{d}{2} + 1\right)}{\pi^{\frac{d}{2}} R_k^d}, \qquad (8)$$

with d the dimension of the space, V_k the volume of the d-ball of radius R_k and $\Gamma(\cdot)$ is the gamma function. The choice of parameter $k = \sqrt{N}$ has been shown to be quasi-optimal in general [17] and is used in the following. This estimator is applied to the sample in the tracker station that is furthest downstream and is represented in the (x, p_x) projection for $(y, p_y) = (0, 0)$ in Figure 8.
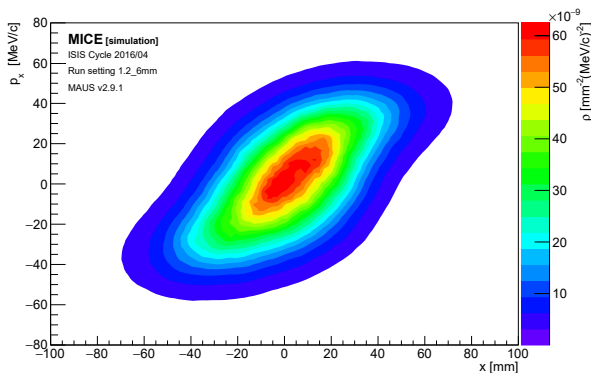

Figure 8: k-Nearest Neighbors estimate of the phase space density in the (x, p_x) projection for $(y, p_y) = (0, 0)$ in the tracker station that is furthest downstream.

This method removes any underlying assumption about a Gaussian core and allows to reconstruct generalized probability contours. The volume of the α-contour is the α-fractional emittance, as defined above. An MC method is used to reconstruct the volume of a contour: select the densest fraction α of the input points and record the level of the lowest point, ρ_α. Sample N random points uniformly distributed inside a box that encompasses the contour and record the amount, N_α, that have a density above the level, i.e. $\rho > \rho_\alpha$. The volume of the contour is simply $\epsilon_\alpha = N_\alpha V_{box}/N$, with V_{box} the volume of the 4-box. The 9 %-contour volume evolution is represented in Figure 9. The estimated relative emittance change with this technique is -7.97 ± 1.63 %.
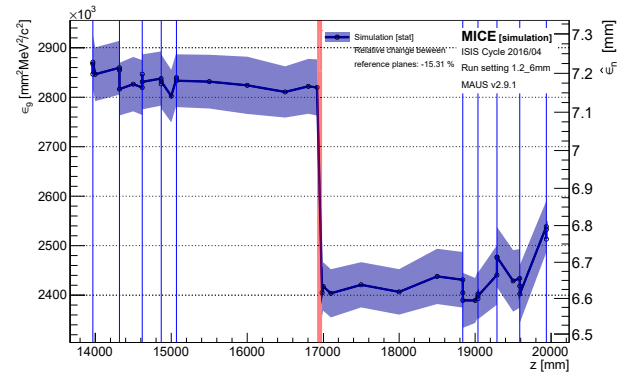

Figure 9: 9 %-contour volume evolution through the MICE cooling channel.

CONCLUSION

While the traditional normalized RMS emittance measurement is vulnerable to transmission losses and non-linearities in the particle ensemble, density estimation techniques provide the most viable option to recover quantitative cooling measurements. Amplitude-based techniques – subemittance and fractional emittance – rely on a well known quantity to select and study an identical fraction of the beam upstream and downstream of the absorber. Nonparametric density estimators allow to go one step further in removing any assumption on the underlying distribution. Both approaches yield compelling results when applied to a poorly transmitted and highly non-linear beams in a realistic simulation of one of the MICE cooling channel settings.

ACKNOWLEDGEMENT

REFERENCES

[1] IDS-NF Collaboration, M. Apollonio *et al.*, "International Design Study for the Neutrino Factory", *Nucl. Phys. Proc. Suppl.* 229-232 (2012) 515–515

[2] Neutrino Factory and Muon Collider Collaboration, M. Alsharoa, *et al.*, "Recent progress in neutrino factory and muon collider research within the Muon collaboration", *Phys. Rev. ST Accel. Beams* 6 (2003) 081001

[3] D. Neuffer, "Principles and Applications of Muon Cooling", *Part. Accel.* 14 (1983) 75–90.

[4] V. Parkhomchuck and A. Skrinsky, "Cooling Methods for Charged Particle Beams", *Rev. Accel. Sci. Tech.* 1 no. 1 (2008) 237

[5] D. Stratakis and R. Palmer, "Rectilinear six-dimensional ionization cooling channel for a muon collider: A theoretical and numerical study" *Phy. Rev. ST Accel. Beams* 18 (2015) 031003

[6] MICE Collaboration, "MICE: An International Muon Ionization Cooling Experiment", MICE Note 21 (2003). `http://mice.iit.edu/micenotes/public/pdf/MICE0021/MICE0021.pdf`.

[7] F. Drielsma, "Results from MICE Step IV", in *Proceedings of "The 2017 European Physical Society Conference on High Energy Physics"* PoS(EPS-HEP2017)534

[8] C. Heidt, "The tracker systems for the muon ionization cooling experiment", *Nucl. Instr. Meth.*, vol. 718 (2014), 560–562.

[9] U. Braver *et al.*, "MICE: the Muon Ionization Cooling Experiment. Step I: First Measurement of Emittance with Particle Physics Detectors", `https://arxiv.org/abs/1110.1813`.

[10] D. Adams *et al.*, "Pion contamination in the MICE muon beam", *JINST* 11 (2016) P03001

[11] D. Adams *et al.*, "Electron-muon ranger: performance in the MICE muon beam", *JINST* 10 (2015) P12012

[12] C.B. Barber, D.P. Dobkin, and H.T. Huhdanpaa, "The Quickhull algorithm for convex hulls", *ACM Trans. on Mathematical Software*, 22(4) (1996) 469-483, `http://www.qhull.org`.

[13] D.W. Hogg, "Data analysis recipes: Choosing the binning for a histogram", `https://arxiv.org/pdf/0807.4820`

[14] Y.P. Mack and M. Rosenblatt, "Multivariate k-nearest neighbor density estimates", *Journal of Multivariate Analysis* Volume 9, Issue 1 (1979), 1–15

[15] M. Browne, "A geometric approach to non-parametric density estimation", *Pattern Recognition* 40(1) (2007), 134–140

[16] M. Browne, "Regularized tessellation density estimation with bootstrap aggregation and complexity penalization", *Pattern Recognition* 45(4) (2012), 1531–1539

[17] D.O. Loftsgaarden and C.P. Quesenberry, "A nonparametric estimate of a multivariate density function", *The Annals of Mathematical Statistics* Vol. 36, No. 3 (1965), 1049–1051